

Selectively doping barlowite for quantum spin liquid: A first-principles study

Zheng Liu,^{1,2} Xiaolong Zou,³ Jia-Wei Mei,⁴ and Feng Liu^{2,5}

¹*Institute for Advanced Study, Tsinghua University, Beijing 100084, China*

²*Department of Materials Science and Engineering, University of Utah, Salt Lake City, Utah 84112, USA*

³*Department of Materials Science and Nanoengineering, Rice University, Houston, Texas 77005, USA*

⁴*Perimeter Institute for Theoretical Physics, Waterloo, Ontario, Canada N2L 2Y5*

⁵*Collaborative Innovation Center of Quantum Matter, Beijing 100084, China*

(Received 1 May 2015; published 18 December 2015)

Barlowite $\text{Cu}_4(\text{OH})_6\text{FBr}$ is a newly found mineral containing Cu^{2+} kagome planes. Despite similarities in many aspects to herbertsmithite $\text{Cu}_3\text{Zn}(\text{OH})_6\text{Cl}_2$, the well-known quantum spin liquid (QSL) candidate, intrinsic barlowite turns out not to be a QSL, possibly due to the presence of Cu^{2+} ions in between kagome planes that induce interkagome magnetic interaction [Phys. Rev. Lett. **113**, 227203 (2014)]. Using first-principles calculation, we systematically study the feasibility of selective substitution of the interkagome Cu ions with isovalent nonmagnetic ions as a function of ion concentration up to the stoichiometric limit. Unlike previous speculation of using larger dopants, such as Cd^{2+} and Ca^{2+} , we identify the most ideal stoichiometric doping elements to be Mg and Zn in forming $\text{Cu}_3\text{Mg}(\text{OH})_6\text{FBr}$ and $\text{Cu}_3\text{Zn}(\text{OH})_6\text{FBr}$ with the highest site selectivity and smallest lattice distortion. The equilibrium antisite disorder in Mg/Zn-doped barlowite is estimated to be one order of magnitude lower than that in herbertsmithite. The single-electron band structure and orbital component analysis show that the proposed selective doping effectively mitigates the difference between barlowite and herbertsmithite.

DOI: [10.1103/PhysRevB.92.220102](https://doi.org/10.1103/PhysRevB.92.220102)

PACS number(s): 75.10.Kt, 71.15.Nc, 71.20.-b

Quantum spin liquid (QSL) represents a new state of matter characterized by long-range entanglement, beyond the conventional symmetry-breaking paradigm [1]. Realizing QSL in real-world materials has been a long-sought goal for decades [2–4]. The most promising candidate so far is herbertsmithite $\text{Cu}_3\text{Zn}(\text{OH})_6\text{Cl}_2$, which realizes the $S = 1/2$ antiferromagnetic (AFM) Heisenberg model on the two-dimensional (2D) kagome lattice [5]. Extensive theoretical studies have suggested that this model is likely to achieve a QSL ground state, despite being close in energy with other competing phases [6–13]. Experiments on herbertsmithite have also shown QSL-like features, such as the absence of any observed magnetic order down to 50 mK [14,15] and an unusual continuum of spin excitations [16]. However, the inevitable Cu/Zn antisite disorder makes the interpretation of experimental data difficult [17]. It remains an open debate whether these defects obscure the intrinsic signals, such as a tiny spin gap that is crucial for the classification of the ground state [18].

Very recently, barlowite $\text{Cu}_4(\text{OH})_6\text{FBr}$ as a new kagome compound was discovered [19]. Its structure closely resembles herbertsmithite, whereas the Cu/Zn antisite disorder is automatically avoided. Therefore, studies on this new material are expected to shed fresh light on understanding the kagome physics and QSL phase. Interestingly, barlowite is diagnosed with a Curie-Weiss constant $\theta_{CW} = -136$ K close to herbertsmithite, yet it undergoes a spin-ordering phase transition at 15 K [20]. The low-temperature magnetic properties were further investigated by combining first-principles calculation with experiments [21]. Since the main structural difference between these two materials is the cations occupying the interkagome sites, i.e., Cu^{2+} and Zn^{2+} in barlowite and herbertsmithite, respectively, it is suggested that substituting the interkagome sites with nonmagnetic ions should tune barlowite into the same phase as herbertsmithite. Specifically,

relatively larger elements, such as Sn and Cd, are speculated as possible candidates for substitution based on the simple argument of lattice spacing of the interkagome sites [20].

In this Rapid Communication, we identify the most promising candidates for realizing the selective doping to form stoichiometric doped barlowite, based on density functional theory (DFT) calculations [22]. We systematically calculate the doping energies and analyze the doping selectivity of a series of nonmagnetic group 2 and 12 elements. Unlike the previous speculation [20], larger dopants are found to have lower site selectivity and tend to distort the kagome plane more than smaller dopants. Most importantly, we identify Mg and Zn to be the most ideal choices of dopants to form stoichiometric $\text{Cu}_3\text{Mg}(\text{OH})_6\text{FBr}$ and $\text{Cu}_3\text{Zn}(\text{OH})_6\text{FBr}$ compounds in the barlowite family, with the highest site selectivity in substituting the interkagome Cu ions and the least lattice distortion in kagome planes. Statistical analysis shows that the equilibrium distribution of Mg/Zn in the Mg/Zn-doped barlowite at the typical growth temperature exhibits a level of antisite disorder significantly lower than that in herbertsmithite. Also, single-electron band structures of intrinsic and doped barlowite are calculated, and discussed in comparison with herbertsmithite.

Figure 1(a) shows the atomic structure of barlowite. Similar to herbertsmithite, it contains Cu^{2+} kagome planes connected by hydroxyls. The difference lies in the interkagome site: in barlowite, there are additional Cu^{2+} ions between the kagome planes, which act as additional spin-1/2 centers and mediate interkagome spin exchange. Therefore, to clarify the different magnetic ground states between barlowite and herbertsmithite, one way is to remove these out-of-plane spins by selective doping. The chosen dopants should be spin zero and isovalent. Using these two criteria, we have considered elements of Mg, Ca, Sr, Ba from group 2 and Zn, Cd from group 12.

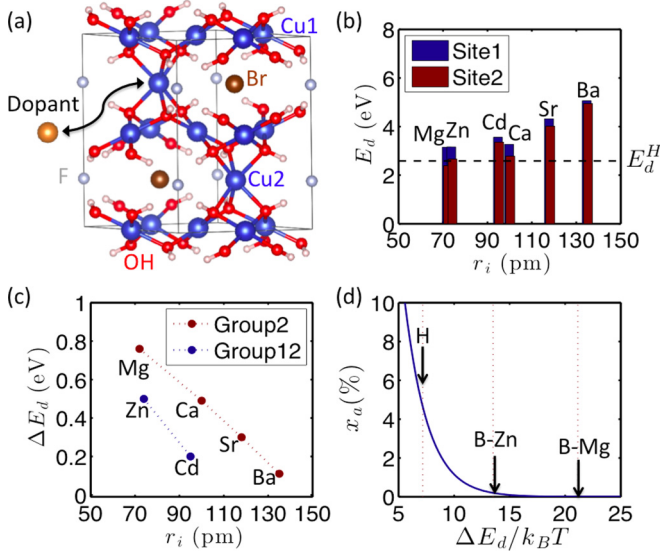
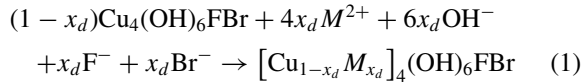


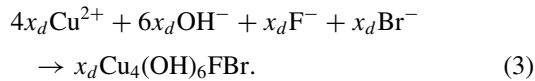
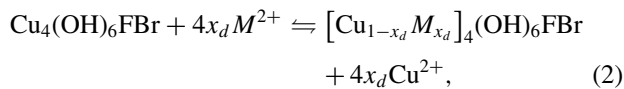
FIG. 1. (Color online) (a) Atomic structure of barlowite, and a schematic illustration of the proposed selective doping. (b) E_d and (c) ΔE_d of different dopants. E_d^H in (b) corresponds to the standard doping energy for the growth of herbertsmithite. The dotted line in (c) only serves as a guide to the eyes. (d) Equilibrium antisite disorder of herbertsmithite (H) and Zn/Mg doped barlowite (B-Zn/Mg).

The doping process is expected to take place by adding dopant ions in solution during the hydrothermal growth. The net reaction equation can be written as



in which M^{2+} denotes the dopants.

Equation (1) can be considered as a combination of two subreactions:



Equation (2) describes the simple substitution process. Then, after the Cu ion is exchanged into the solution, the overall free energy of the system can be lowered by forming more deposits of barlowite [Eq. (3)]. The thermodynamic driving force for doping to proceed is that the extra dopant cations assist more anions to deposit from the solution. Equation (3) is actually nothing but the growth of undoped barlowite as reported in previous experiments [20,21]. Hence, we will focus on evaluating the experimental feasibility of Eq. (2) only.

The central physical quantity we are going to calculate is the standard doping energy E_d as defined by the total energy difference per substitution. According to Eq. (2), E_d consists of two parts: $E_d = \Delta E_B + \Delta \mu_i^0$, where $\Delta E_B = (E_{[\text{Cu}_{1-x_d} M_{x_d}]_4(\text{OH})_6\text{FBr}} - E_{\text{Cu}_4(\text{OH})_6\text{FBr}})/4x_d$ is the energy change of barlowite after doping and $\Delta \mu_i^0 = \mu_{\text{Cu}^{2+}}^0 - \mu_{M^{2+}}^0$ is the difference of the standard chemical potential [23]. There are two

TABLE I. A comparison of structural parameters between theory and experiment.

Barlowite	Expt. [20]	Expt. [21]	Cal.
Lattice a/b (Å)	6.68	6.80	6.73
Lattice c (Å)	9.31	9.31	9.47
Angle Cu1-O-Cu1	117.4°	117°	117.3°
Angle Cu1-O-Cu2	95.8°		96.6°

inequivalent doping sites: Cu1 is in the kagome plane; Cu2 is between the kagome planes. We use E_{d1} and E_{d2} to differentiate these two types of doping energies. Their difference $\Delta E_d(x_d) = E_{d1}(x_d) - E_{d2}(x_d)$ tells the site preference for dopants, i.e., defines the degree of selective doping.

Our calculation on ΔE_B is carried out using the VASP package [24], which solves the DFT Hamiltonian self-consistently using the plane-wave basis together with the projector augmented wave method [25]. A plane-wave cutoff of 500 eV is enforced. The self-consistent iterations are converged to 0.1 meV precision of the total energy. We employ the generalized gradient approximation as parametrized by Perdew, Burke, and Ernzerhof for the exchange-correlation functional [26], which is known to satisfactorily describe ionic bonding and cohesive energy even for transition elements. The atomic coordinations are fully relaxed until the forces are less than 0.05 eV/Å. The total-energy integration over the Brillouin zone is obtained on a Γ -centered $2 \times 2 \times 2$ k mesh. A spinless calculation on the structure and total energy is reasonable, considering (1) barlowite stays in the paramagnetic phase above 15 K (1 meV) [20,21], and (2) the Dzyaloshinskii-Moriya interaction arising from spin-orbit coupling is estimated to be of the order of 1 meV [21]. As a benchmark, Table I summarizes the calculated structural parameters of undoped barlowite, which agree with the experimental results well. Note that we do not intend to discuss strong correlation effects associated with the Cu 3d orbitals within this methodology.

To simulate doping, we construct a $2 \times 2 \times 1$ supercell containing 24 in-plane Cu1 sites and eight interkagome Cu2 sites. We will first calculate E_d of different isovalent nonmagnetic ions by replacing one of the Cu^{2+} and fixing the lattice constant to the experimental value, which serves to sort out the most ideal dopants. After that, we will perform fully relaxed calculation and progressively increase the concentration of the most ideal dopants to confirm the structural stability and understand the change of the electronic structure up to the stoichiometric limit.

Figure 1(b) shows the calculated E_d as a function of the ionic radius [27]. Note that Mg^{2+} and Zn^{2+} are close in radius to Cu^{2+} (73 pm), while the other ions are larger. As a reference, we have also calculated the standard doping energy for the growth of herbertsmithite [E_d^H in Fig. 1(b)] as described by the following equation: $[\text{Cu}_{3+x_d} \text{Zn}_{1-x_d}](\text{OH})_6\text{Cl}_2 + x_d \text{Zn}^{2+} \rightleftharpoons \text{Cu}_3 \text{Zn}(\text{OH})_6\text{Cl}_2 + x_d \text{Cu}^{2+}$. The positive doping energy acts as a reaction barrier, which limits the kinetics of Eq. (1). The value of E_{d2} for Zn is found almost the same as E_d^H , again reflecting the similarities between barlowite and herbertsmithite. E_d typically increases with the ionic radius: Mg is even easier to

substitute Cu than Zn, while larger dopants are more difficult. The kagome-site doping energy (E_{d1}) is always higher than the interkagome-site doping energy (E_{d2}), indicating that the latter is the preferred site for doping. The preference for dopants to occupy the interkagome site provides exactly the type of doping selectivity we need. To better show the energy difference, in Fig. 1(c), we plot $\Delta E_d = E_{d1} - E_{d2}$ as a function of ion radius. ΔE_d decreases when r_i increases, suggesting that large dopants actually have lower site preference, hence are more difficult to achieve stoichiometric doping. This invalidates the previous speculation [20].

The basic features of ΔE_d can be understood by examining the chemical environment of the two Cu sites [Fig. 1(a)]: the Cu1 site is surrounded by four hydroxide ligands in a planar square geometry; the Cu2 site is surrounded by six hydroxide ligands in a trigonally compressed octahedral geometry. For Mg and Zn that have a similar ionic radius to Cu, ΔE_d has an electronic origin. Like in herbertsmithite, the d^9 open-shell Cu^{2+} ion can take advantage of the lower symmetry of the Cu1 site to reduce the overall energy [5]. Letting the closed-shell dopant substitute the Cu2 site thus gives relatively smaller doping energy. As the dopant size increases, the size effect also kicks in. The energy cost for the dopants staying at the Cu2 site grows faster than staying at the Cu1 site due to the higher coordination number. Consequently, within each group, ΔE_d decreases monotonously. The elements from two groups are not on the same curve, because the outermost shells of group 2 and 12 ions are p^6 and d^{10} , respectively. Thus, they will exhibit different bonding energy with the ligands.

Another problem for the large dopants is identified after fully relaxing the lattice volume and geometry. While interkagome doping maintains the original lattice symmetry, the in-plane doping distorts the lattice from hexagonal to triclinic, breaking the perfect kagome plane and lowering the in-plane doping energy. Consequently, ΔE_d becomes smaller. This effect becomes very significant for larger dopants. For example, for Cd^{2+} and Ca^{2+} , ΔE_d decreases from 0.20 and 0.50 eV to -0.12 and 0.11 eV, respectively. It means that upon doping, a large fraction of dopants will substitute the in-plane sites, which in turn distorts the lattice and hinders stoichiometric selective doping. In contrast, for Mg^{2+} and Zn^{2+} , which have similar radius to Cu^{2+} , this problem does not occur: ΔE_d decrease from 0.76 and 0.50 eV to 0.72 and 0.46 eV, respectively, which are still sufficiently large to suppress in-plane doping. Therefore, we conclude that for our purpose Mg^{2+} and Zn^{2+} are the most ideal dopants.

To further examine whether the selective doping of Mg/Zn at the interkagome sites can sustain up to the stoichiometric limit to form $\text{Cu}_3\text{Mg}(\text{OH})_6\text{FBr}$ and $\text{Cu}_3\text{Zn}(\text{OH})_6\text{FBr}$ compounds, we proceed by progressively increasing the amount of interkagome dopants. E_d is found to be nearly independent of the doping concentration (x_d). This property indicates that the interaction between the dopants is weak, which is important for reaching the stoichiometric limit. Otherwise, dopants may form clusters or hinder further doping process. We have also checked that the lattice and Cu kagome planes in $\text{Cu}_3\text{Mg}(\text{OH})_6\text{FBr}$ and $\text{Cu}_3\text{Zn}(\text{OH})_6\text{FBr}$ remain stable under structural relaxation.

It is worth making some comparison to herbertsmithite within the present methodology. The first critical issue is the

degree of equilibrium antisite disorder in the two systems. The effect of Cu/Zn antisite disorder in herbertsmithite has been a long-lasting debate [18]. Such disorder is inevitable in doped barlowite as well, because it leads to an increase of the configuration entropy. Under constant temperature and volume, the equilibrium is reached by minimizing the free energy $F(x_a) = E(x_a) - TS(x_a)$ with respect to the antisite concentration x_a . Without loss of generality, it is convenient to set $E(0) = S(0) = 0$ for the stoichiometric systems. Accordingly, when x_a pairs of Mg(Zn) and Cu per $\text{Cu}_3\text{M}(\text{OH})_6\text{FBr}$ unit switch sites, the energy increase is simply $E(x_a) = x_a \Delta E_d$, given that the interaction between the dopants is weak. The entropy increase per $\text{Cu}_3\text{M}(\text{OH})_6\text{FBr}$ unit can be analytically derived as $S(x_a) = -k_B \ln[(3 - x_a)^{3-x_a} (1 - x_a)^{1-x_a} x_a^{2x_a}]$ (see Appendix for details). The minimal point of $F(x_a)$ is calculated numerically, which can be expressed as a function of $\Delta E_d/k_B T$ [Fig. 1(d)]. By using the calculated values of ΔE_d (Mg: 0.72 eV; Zn: 0.46 eV) and the experimental growth temperature ($T = 393$ K) [20], the antisite disorder in Mg/Zn doped barlowite is predicted to be below 0.1%. For comparison, we have also calculated $\Delta E_d = 0.30$ eV for herbertsmithite and with $T = 483$ K [5], the equilibrium disorder is calculated to be 5%, comparable to the experimental estimation [18]. Therefore, the degree of antisite disorder in the doped barlowite is expected to be at least one order of magnitude lower than that in herbertsmithite, owing to higher ΔE_d as well as lower growth temperature. This difference can be significant to help clarify the effects of disorder on the QSL phase.

Secondly, we do a comparison of single-electron band structure. Figure 2 shows the band structures of herbertsmithite, undoped and doped ($x_d = 1$) barlowite marked with orbital compositions. Despite the absence of strong-correlation effects, the DFT single-electron band structure properly describes single-electron hopping processes, which serve as the guide to the AFM superexchange. For herbertsmithite, there

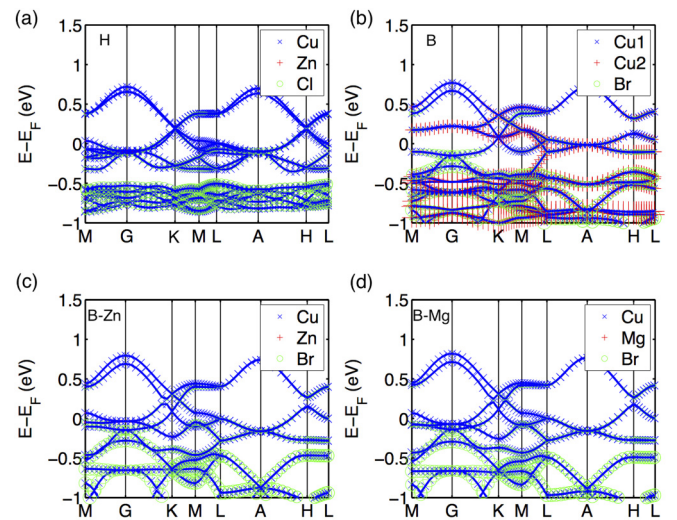


FIG. 2. (Color online) Orbital resolved single-electron band structure of herbertsmithite (H), barlowite (B), and Zn/Mg doped barlowite (B-Zn/Mg). The marker size reflects the weight of atomic composition.

is a set of bands around the Fermi level (between -0.5 and 0.75 eV), gapped from the underlying valence bands [28]. These bands primarily arise from Cu [blue cross in Fig. 2(a)] and the adjacent O (not shown), exhibiting the typical features of nearest-neighbor hopping on a 2D kagome lattice [29]. For barlowite [Fig. 2(b)], around 0.5 eV the band dispersion is similar to that in herbertsmithite with the band composition primarily from the in-plane Cu, indicating similar hopping amplitude within the kagome planes. This is in agreement with the experimental fact that the Curie-Weiss constant for herbertsmithite and barlowite is close [20]. However, around the Fermi level, interkagome Cu not only contributes extra bands, but also strongly mix with the Cu1 bands. This result suggests considerable coupling between Cu1 and Cu2, as pointed out by previous studies [20,21]. The effect of replacing Cu2 with Zn or Mg is remarkable [Figs. 2(c) and 2(d)]. After doping, the complexities of interkagome coupling are removed. Both Zn and Mg states are far from the Fermi level, leaving clean Cu1 bands around the Fermi level. The overall band dispersion also becomes closer to herbertsmithite. The energy states below the Fermi level contain contribution from the halogen atoms, i.e. Cl and Br in herbertsmithite and barlowite, respectively. We note that both Cl^- and Br^- are spin zero and far away from the superexchange path between Cu1 ions. Therefore, these orbitals do not play an important role in the magnetic properties.

In conclusion, based on the DFT calculation, we identify $\text{Cu}_3\text{Mg}(\text{OH})_6\text{FBr}$ and $\text{Cu}_3\text{Zn}(\text{OH})_6\text{FBr}$ as the most promising targets to realize the stoichiometric doped barlowite. The distinct advantages include no lattice distortion, high site selectivity, and low antisite disorder. The standard doping energy is comparable to (for Zn) or even lower (for Mg) than that for growing herbertsmithite. Therefore, these targets may be readily synthesized using similar experimental conditions as used for herbertsmithite. The remaining open question is how the doped barlowite behaves magnetically under low temperature: will it be tuned into the same phase as

herbertsmithite or stay as the undoped barlowite? For either case, the effective doping of this new material as we propose here serves as a useful guide to future experiments in a pursuit to reveal key factors towards QSL.

Z.L. is supported by Tsinghua University Initiative Scientific Research Program. Z.L. and F.L. also acknowledge support from DOE-BES (Grant No. DE-FG02-03ER46027). Work at Rice University (X.Z. and discussions with B.I. Yakobson) is supported by DoD MURI program (Grant No. W911NF-11-1-0362). J.-W.M. is supported by the Government of Canada through Industry Canada and by the Province of Ontario through the Ministry of Research.

APPENDIX: CONFIGURATION ENTROPY OF ANTISITE DISORDER

Let us consider an ensemble of N units of $\text{Cu}_3M(\text{OH})_6\text{FBr}$ or $\text{Cu}_3M(\text{OH})_6\text{Cl}_2$. If there is N_a pairs of M and Cu switch sites, the antisite disorder concentration is defined by $x_a = N_a/N$. The configuration number Ω is given by

$$\Omega = \frac{(3N)!}{N_a!(3N - N_a)!} \times \frac{N!}{N_a!(N - N_a)!} \quad (\text{A1})$$

When the values of N and N_a are large, the Sterling's approximation gives

$$\begin{aligned} \ln \Omega &= 3N \ln(3N) - N_a \ln(N_a) - (3N - N_a) \ln(3N - N_a) \\ &\quad + N \ln N - N_a \ln N_a - (N - N_a) \ln(N - N_a). \end{aligned} \quad (\text{A2})$$

The configuration entropy per unit is then

$$\begin{aligned} S &= \frac{k_B}{N} \ln \Omega \\ &= -k_B \ln \left[(3 - x_a)^{3-x_a} (1 - x_a)^{1-x_a} x_a^{2x_a} \right] + 3 \ln 3. \end{aligned} \quad (\text{A3})$$

-
- [1] X.-G. Wen, *Quantum Field Theory of Many-Body Systems from the Origin of Sound to an Origin of Light and Electrons* (Oxford University Press, New York, 2004).
- [2] P. W. Anderson, *Mater. Res. Bull.* **8**, 153 (1973).
- [3] L. Balents, *Nature (London)* **464**, 199 (2010).
- [4] P. A. Lee, *Science (New York)* **321**, 1306 (2008).
- [5] M. P. Shores, E. A. Nytko, B. M. Bartlett, and D. G. Nocera, *J. Am. Chem. Soc.* **127**, 13462 (2005).
- [6] S. Sachdev, *Phys. Rev. B* **45**, 12377 (1992).
- [7] P. Lecheminant, B. Bernu, C. Lhuillier, L. Pierre, and P. Sindzingre, *Phys. Rev. B* **56**, 2521 (1997).
- [8] S. Ryu, O. I. Motrunich, J. Alicea, and M. P. A. Fisher, *Phys. Rev. B* **75**, 184406 (2007).
- [9] Y. Ran, M. Hermele, P. A. Lee, and X.-G. Wen, *Phys. Rev. Lett.* **98**, 117205 (2007).
- [10] Y.-M. Lu, Y. Ran, and P.-A. Lee, *Phys. Rev. B* **83**, 224413 (2011).
- [11] S. Yan, D. A. Huse, and S. R. White, *Science* **332**, 1173 (2011).
- [12] Y. Iqbal, F. Becca, S. Sorella, and D. Poilblanc, *Phys. Rev. B* **87**, 060405 (2013).
- [13] Y. Iqbal, D. Poilblanc, and F. Becca, *Phys. Rev. B* **89**, 020407 (2014).
- [14] J. S. Helton, K. Matan, M. P. Shores, E. A. Nytko, B. M. Bartlett, Y. Yoshida, Y. Takano, A. Suslov, Y. Qiu, J. H. Chung *et al.*, *Phys. Rev. Lett.* **98**, 107204 (2007).
- [15] P. Mendels, F. Bert, M. A. de Vries, A. Olariu, A. Harrison, F. Duc, J. C. Trombe, J. S. Lord, A. Amato, and C. Baines, *Phys. Rev. Lett.* **98**, 077204 (2007).
- [16] T.-H. Han, J. S. Helton, S. Chu, D. G. Nocera, J. A. Rodriguez-Rivera, C. Broholm, and Y. S. Lee, *Nature (London)* **492**, 406 (2012).
- [17] A. Olariu, P. Mendels, F. Bert, F. Duc, J. C. Trombe, M. A. de Vries, and A. Harrison, *Phys. Rev. Lett.* **100**, 087202 (2008).
- [18] P. Mendels and F. Bert, *J. Phys.: Conf. Ser.* **320**, 012004 (2004).
- [19] P. Elliott, M. A. Cooper, and A. Pring, *Mine. Mag.* **78**, 1755 (2014).

- [20] T.-H. Han, J. Singleton, and J. A. Schlueter, *Phys. Rev. Lett.* **113**, 227203 (2014).
- [21] J. O. Jeschke, F. Salvat-Pujol, E. Gati, N. H. Hoang, B. Wolf, M. Lang, J. A. Schlueter, and R. Valenti, *Phys. Rev. B* **92**, 094417 (2015).
- [22] R. O. Jones and O. Gunnarsson, *Rev. Mod. Phys.* **61**, 689 (1989).
- [23] G. Job, *Table of Chemical Potentials*, Eduard-Job Foundation for Thermo and Matter Dynamics, online database: <http://www.job-stiftung.de/index.php?data-collection>.
- [24] G. Kresse and J. Furthmuller, *Phys. Rev. B* **54**, 11169 (1996).
- [25] G. Kresse and D. Joubert, *Phys. Rev. B* **59**, 1758 (1999).
- [26] J. P. Perdew, K. Burke, and M. Ernzerhof, *Phys. Rev. Lett.* **77**, 3865 (1996).
- [27] R. D. Shannon, *Acta. Crystallogr., Sect. A: Cryst. Phys., Diffraction, Theor. Gen. Crystallogr.* **32**, 751 (1976).
- [28] H. O. Jeschke, F. Salvat-Pujol, and R. Valenti, *Phys. Rev. B* **88**, 075106 (2013).
- [29] Z. Liu, F. Liu, and Y.-S. Wu, *Chin. Phys. B* **23**, 77308 (2014).